Improved Planar InAs Avalanche Photodiodes With Reduced Dark Current and Increased Responsivity

Leh Woon Lim, Chee Hing Tan, *Senior Member, IEEE*, Jo Shien Ng, *Member, IEEE*, Jonathan D. Petticrew, *Student Member, IEEE*, and Andrey B. Krysa

***Abstract*—Indium Arsenide (InAs) infrared photodiodes provide high quantum efficiency in the wavelength range of 1.0–3.0 μm. Planar diode configuration has been adopted to reduce surface leakage. In this work, new fabrication procedures for planar InAs avalanche photodiodes (APDs) are reported. Beryllium (Be) ions were implanted into InAs at a relatively low energy of 34 keV. Effects of duration of post implant annealing on the electrical characteristics of InAs APDs were investigated. It was found that a combination of post implant annealing at 500 °C for 15 min and a shallow surface etch produces planar APDs with good characteristics (room temperature dark current density of 0.52 A/cm^2 at −0.2 V and external quantum efficiency of 51% at 1520 nm at −0.3 V). These represent a 3 times reduction in dark current and 1.4 times increase in responsivity, compared to earlier Be-implanted planar InAs APDs. The APDs' avalanche gain characteristics remain similar to those from earlier reports, with a gain of 4 at a relatively low operating bias of 5 V. This suggests the potential of integrating InAs APDs with low voltage readout integrated circuits (ROIC) for development of infrared imaging arrays. The data reported in this paper is available from the ORDA digital repository (DOI: 10.15131/shef.data.6955037).**

***Index Terms*—Avalanche photodiodes, Indium Arsenide, infrared detectors.**

I. Introduction

INDIUM Arsenide (InAs) has a bandgap of 0.34 eV at room temperature, exhibiting a peak detection wavelength of 3.35 μm, and a cutoff (50% of the peak response) wavelength of 3.55 μm [1]. Therefore, InAs is well suited for applications at infrared (IR) wavelengths from 1.0 to 3.0 μm such as remote gas sensing [2], shortwave IR imaging [3] and light detection and ranging (LiDAR) [4]. For applications where the incoming photons are sparse, the weak photocurrent can be amplified by avalanche multiplication in avalanche photodiodes (APDs). As a result, using an APD in an optical receiver can significantly improve the receiver's signal-to-noise ratio (SNR), when the receiver's noise is dominated by the electronics.

Manuscript received December 7, 2018; revised March 1, 2019; accepted March 11, 2019. Date of publication March 15, 2019; date of current version April 17, 2019. This work was supported by the UK Defense Science and Technology Laboratory under Grant DSTLX1000108233. *(Corresponding author: Leh Woon Lim.)*

The authors are with the Department of Electronic and Electrical Engineering, University of Sheffield, Sheffield S1 3JD, U.K. (e-mail: lwlim1@sheffield.ac.uk; c.h.tan@sheffield.ac.uk; j.s.ng@sheffield.ac.uk; jpetticrew1@sheffield.ac.uk; a.krysa@sheffield.ac.uk).

Color versions of one or more of the figures in this paper are available online at http://ieeexplore.ieee.org.

Digital Object Identifier 10.1109/JLT.2019.2905535

For detection of IR wavelengths above 1.55 μm, the best APD performance has been achieved using Mercury Cadmium Telluride (HgCdTe). The HgCdTe APDs show very high gain, and very low excess noise factors of 1.0 to 1.5 [5]. They have also been demonstrated as functional 2-dimensional arrays [6]. However, most HgCdTe APDs are grown on small, expensive substrates. When coupled with relatively low manufacturing yield [7], limited suppliers [8] and cryogenic operating temperatures [9], the use of HgCdTe APDs tends to be limited to high-end instruments for space and military applications. In addition, the move towards a Hg-free economy [10] may affect future supply chain for HgCdTe. Therefore, III-V APDs with mature growth and fabrication techniques can be attractive alternatives to HgCdTe APDs.

InAs APDs have demonstrated impact ionization properties that are similar to HgCdTe APDs. InAs APDs exhibit an excess noise factor <2 [11], gain-independent bandwidth [12] and a high quantum efficiency in the midwave IR wavelengths [1]. The low excess noise and gain-independent bandwidth of InAs APDs are achieved because only electrons are capable of initiating impact ionization events [11]. The electron-dominated avalanche gain also ensures termination of the avalanche process within two carrier transit times. Hence the timing jitter is expected to be small, as indicated by LiDAR measurements with picosecond resolution using InAs APDs operated at room temperature [13].

To date, most reports of InAs APDs are based on mesa APDs fabricated using wet chemical etching. Mesa InAs APDs use surface passivation techniques to suppress surface leakage mechanisms [14] and achieve bulk-dominated dark currents at room temperature. Analyses of the temperature dependence of dark current showed that diffusion current is dominant at temperatures above 200 K [15]. To obtain high gain at a given reverse bias, thick intrinsic regions in p-i-n InAs APDs are required [16]. In structures optimized for achieving high gain, devices may be up to 10 μm thick [17]. However, defects arising from dangling bonds along the etched surfaces risk device failure (due to the presence of a high electric field in the avalanche region). Sidewall passivation in thick mesa structures is impractical and complicates the fabrication process. Furthermore, mesa InAs diodes fabricated using chemical wet etching produces varying bevel angles (depending on the etchants used), limiting the fill factor of small area diode arrays. Planarization by ion implantation or selective area diffusion can remove the aforementioned complexities in the production of InAs diodes. Hence, planar

TABLE I
INAS SAMPLE DETAILS

Sample	Implantation and device topology	Annealing duration (minutes)	Additional surface processing
A0	Blanket implantation; mesa devices	0	-
A1		15	-
A2		30	-
A3		60	-
B0	Patterned implantation; planar devices	15	-
B1			HF clean
B2			Shallow surface etch

structures are preferred for simpler device processing as well as increased reliability and uniformity [18]. Using Beryllium (Be) ion implantation (at energies of 70 and 200 keV), planar InAs APDs have been demonstrated with bulk-dominated dark current and high avalanche gain [19], [20]. However their dark current densities at room temperature are ∼10 times higher than those of mesa InAs APDs, suggesting that the Be ion implantation procedures may require optimization.

In this work, we report planar InAs APDs produced using Be ion implantation at a lower implant energy of 34 keV. Post-implant annealing conditions have also been investigated. A room temperature dark current density of 0.52 A/cm^2 at −0.2 V and an external quantum efficiency of 51% at 1520 nm at −0.3 V were achieved with these Be-implanted planar InAs APDs. The dark current is 3 times smaller and the responsivity is 1.4 times greater, compared to previous planar APDs [19].

II. EXPERIMENTAL DETAILS

An InAs wafer with a 7 μm i-layer and a 1 μm highly doped n-layer was used in this work. The wafer was grown by Metalorganic Vapor Phase Epitaxy (MOVPE) in a horizontal flow reactor. Two samples, A and B, were prepared for Be ion implantation. A thin SiO_2 protective layer was deposited using Plasma Enhanced Chemical Vapor Deposition (PECVD) on both samples. The SRIM software package was employed to predict the distribution profile of Be ion implantation in InAs [21]. The simulation estimated an implant energy of 34 keV was required to achieve a target depth of 100 nm. The ion implantation on both samples was therefore carried out at 34 keV, with a dosage of 2×10^{14} cm^{-2}, at room temperature, and a tilt angle of 7° to minimize channeling effects. The sample details are summarized in Table I.

Sample A was implanted without a protective mask (blanket implant), then cleaved into four pieces and fabricated into mesa diodes to study the effects of post-implant annealing. The first sample, A0 was not annealed to serve as a reference. The other samples, A1, A2 and A3, were annealed at 500 °C in a nitrogen-rich furnace for durations of 15, 30 and 60 minutes respectively. After annealing, the SiO_2 was removed using a 10% buffered hydrofluoric acid (HF) etch. Mesa diodes of varying sizes were fabricated from these samples using wet etching [15]. Dark current data from mesa diodes of samples A0 to A3 were then used to select suitable annealing conditions for planar diode fabrication.

Sample B has implantation windows defined by patterned photoresist. Annealing conditions selected from samples A0 to A3 were applied to sample B. To study the effects of surface treatments on planar samples, sample B was cleaved into two smaller pieces, sample B1 (with a 10% buffered HF etch for 30 s) and B2 (shallow surface etch). Sample B2 was etched with a 1:1:1 mixture of phosphoric acid (85%), hydrogen peroxide (30%) and de-ionized water for 10 seconds, followed by a finishing etch with a 1:8:80 mixture of sulphuric acid (95%), hydrogen peroxide (30%) and de-ionized water for 30 seconds.

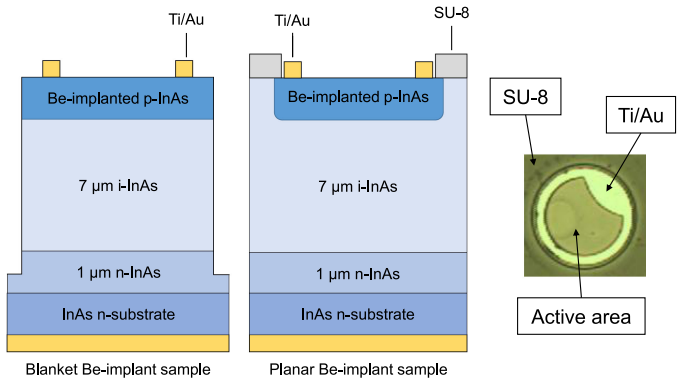

Fig. 1. Schematic diagram of the blanket implanted mesa APDs (left), planar InAs APDs (center) and micrograph of planar InAs APD with SU-8 (right).

The surface around the planar APDs was passivated with SU-8 [15]. SU-8 is an epoxy-based negative photoresist used in microelectronics applications with good chemical properties, mechanical robustness and is transparent to wavelengths above 360 nm. No antireflection coating was deposited on the optical window. A schematic diagram of the diodes and a micrograph is shown in Fig. 1.

The dark current-voltage characteristics were measured using a HP4140B Picoammeter/DC Voltage Source. To verify whether the dark current is dominated by bulk mechanisms, dark currents measured from diodes with different diameters were normalized to the respective diode areas to produce the dark current density. A good agreement between dark current density values from different diode diameters indicates dominance of bulk dark current over surface leakage current. Responsivity measurements were performed using a He-Ne laser of 1520 nm wavelength and the laser spot was confined to the active optical window to ensure pure electron injection. For each sample, dark current characteristics and responsivity were measured on three to five devices per device size for three sizes. In addition, device fabrication for all samples, except samples A0 and B0, was repeated to check reproducibility.

III. RESULTS AND DISCUSSION

The room temperature dark current density-voltage (J-V) characteristics of mesa diodes fabricated from samples A0 to A3 are shown in Fig. 2 (top). The unannealed diodes (sample A0) lack diode rectifying behavior. This is in contrast with the data from the annealed samples A1 to A3, showing clear rectifying behavior (a rapid turn on in the forward bias and a well-defined saturation current in the reverse bias). Comparison of current densities from diodes with different diameters

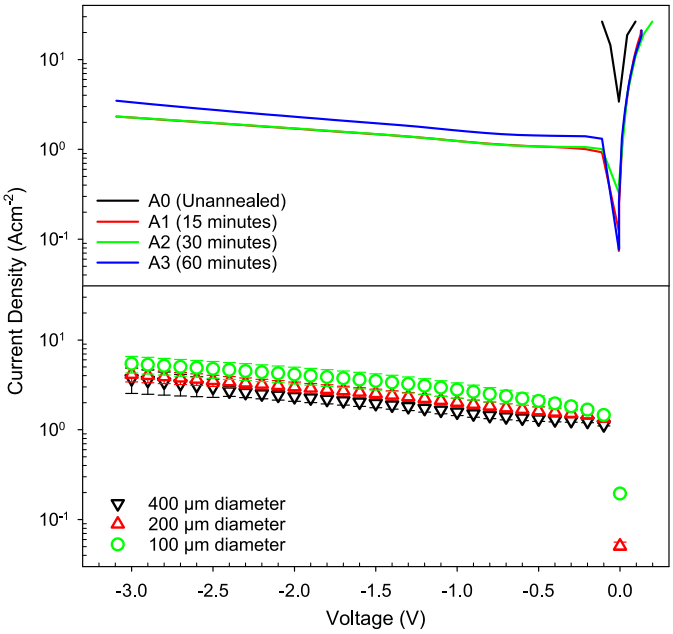

Fig. 2. (Top) Room temperature dark current density characteristics of 220 μm diameter mesa APDs from samples A1, A2 and A3. Data from sample A0 is included for comparison. (Bottom) Room temperature dark current density characteristics of sample B (prior to surface treatment) with diameters of 100, 200 and 400 μm, annealed for 15 minutes. The standard deviation is represented as error bars.

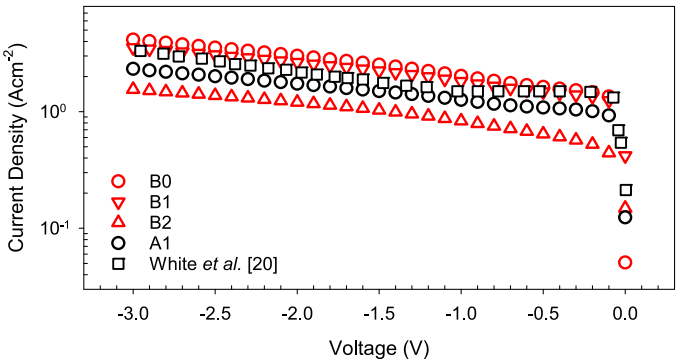

Fig. 3. Dark current density comparison of planar InAs APDs with (samples B1 and B2) and without (sample B0) surface treatments. Data from sample A1 and previous planar InAs APDs [20] are included.

indicates that the dark current is predominantly bulk at room temperature. The recorded current densities at -0.2 V from nominally 220 μm diameter diodes for a given sample are 1.01, 1.06, and 1.40 A/cm^2 for samples A1, A2, and A3 respectively. The dark current density appears to be marginally higher for A3. Based on these values, a 15 minutes anneal is deemed sufficient to achieve good diode behavior and was adopted for subsequent planar APD fabrication. Further annealing does not offer significant reduction in the dark current.

Similar J-V analyses were carried out for the planar APDs without any surface treatment (sample B0). The dark J-Vs are in good agreement, as shown in Fig. 2 (bottom). The dark current density of 200 μm diameter devices is 1.46 A/cm^2 at -0.2 V.

Average value of responsivity at 1520 nm wavelength for sample B0 is 0.48 A/W at -0.3 V, corresponding to 39% external quantum efficiency. This is much lower than the ideal external quantum efficiency, which is 70% by taking into account a 30% reflection loss (caused by a lack of antireflection coating on the optical window). With a total thickness of 8 μm InAs material grown on InAs substrate in our samples, the 1520 nm wavelength light is expected to be fully absorbed (assuming an absorption coefficient of 1.1×10^4 cm^{-1} [22]). Hence the discrepancy between our data of 39% and the expected value of 70% suggests there are additional loss mechanisms in our APDs. A possible mechanism is significant recombination of photogenerated carriers near the top surface, arising either from surface contamination or implantation damage [23].

To investigate the loss mechanism(s), the J-V data from samples B0, B1 and B2 are compared in Fig. 3. Data from mesa APDs of this work (sample A1) and an earlier planar InAs APD [17] are included in the comparison of the five data sets presented in Fig. 3. Sample B2 which has a shallow etch as its surface treatment exhibits the lowest dark current density, 0.52 A/cm^2 at -0.2 V, which is a factor of 3 lower than earlier reports using higher ion implantation energies of 70 and 200 keV [20]. The statistical fluctuations in devices measured from sample B0 and B2 are minimal across the voltage range measured. Therefore the reduced dark current in sample B2 is attributed to reduced surface leakage in the diodes. It has also been observed in other IR photodiodes, such as HgCdTe and InSb, that dark current reduces following a shallow etch [24], [25].

In addition to reducing the dark current, the surface treatments were also found to improve the device responsivity. The measured responsivity values at 1520 nm wavelength of samples B0, B1 and B2 are 0.48, 0.55 and 0.62 A/W at -0.3 V, respectively. This suggests reduced surface recombination in samples B1 and B2, compared to B0. For sample B2, its responsivity of 0.62 A/W, which corresponds to 51% external quantum efficiency, is 1.4 times higher than that from earlier planar InAs APDs made with higher ion implantation energies [19]. Its improvement over sample B1 in terms of responsivity may be due to removal of damage created by ion implantation and the addition of an optimized antireflection coating will increase the quantum efficiency.

The spatial uniformity of responsivity was inspected by raster-scanning a laser across a 400 μm diameter planar diode from sample B2 at room temperature. The measured responsivity is shown in Fig. 4. We observed that the responsivity decreases as the laser spot moves away from the metal contact, leading to approximately 20% smaller responsivity at the center of the planar APD. This non-uniformity in responsivity is also reported in commercial InAs photodiodes from Teledyne Judson [26] and Hamamatsu Photonics [27], whose data are shown in a comparison of relative responsivity in Fig. 5. In the comparison, we have also included data from our mesa InAs APDs grown using MOVPE, which provide more uniform responsivity. The discrepancy between our planar and mesa InAs APDs may be due to differences in p-type dopant activation in the

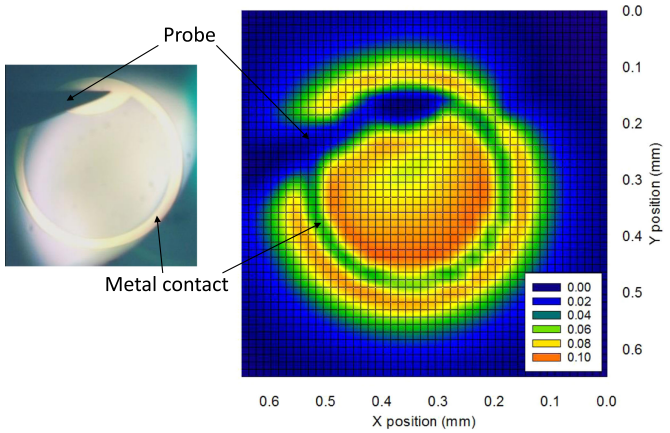

Fig. 4. A diagram of a 400 μm diameter planar APD from sample B2 under probing and its spatial responsivity scan at -0.1 V using a 633 nm wavelength laser.

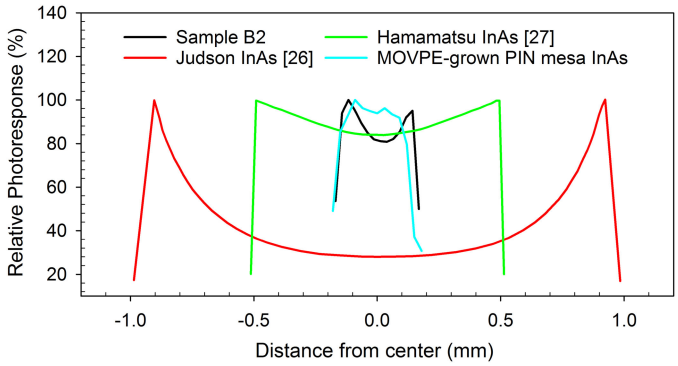

Fig. 5. Comparison of relative photoresponse across the active optical window of planar APDs of this work (sample B2), mesa InAs APD, and commercial planar InAs photodiodes [26], [27].

two APDs. MOVPE-grown mesa InAs APDs may have more uniform activation of Zn dopant atoms in their p-layer, leading to spatially uniform responsivity. The post-implant annealing conditions used for our planar APDs may not have activated all the implanted Be dopant atoms. Another possible reason is the recombination of generated photocarriers due to a shunting effect [26].

Using three selected planar APDs with diameters of 200 μm from sample B2, room temperature gain versus reverse bias characteristics for the illumination wavelength of 633 and 1520 nm was obtained. The mean gain is plotted in Fig. 6, together with values reported in literature for InAs mesa and planar APDs [15], [20], [28]. The APDs reported by Sun *et al*. [28] and White *et al*. [20] have avalanche region widths of 6 and 8 μm respectively, similar to that of our planar APDs (7 μm). Hence all three APDs exhibit similar gain characteristics. For a given reverse bias, our APD's gain is greater than that of mesa APDs with a 4.5 μm wide avalanche region [15]. This is expected since the avalanche gain in a single carrier ionization process is approximately given by $M = \exp(\alpha W)$, where α is the ionization coefficient and W is the avalanche region width. For our planar InAs APD, a gain of

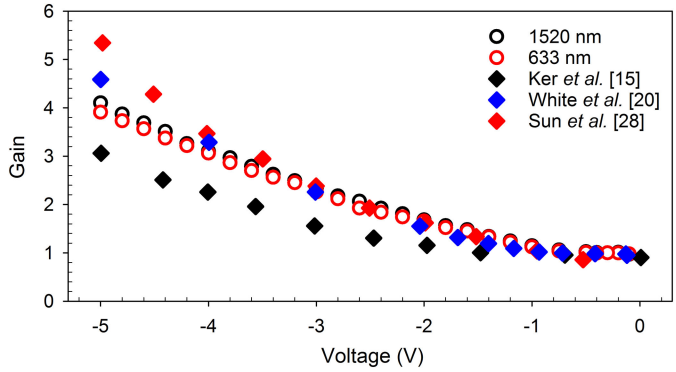

Fig. 6. Gain of planar APDs from sample B2 at different wavelengths along with comparisons to published results on mesa InAs APDs and planar InAs APDs.

4 was obtained at -5 V, making InAs an attractive APD technology for integration with low voltage readout IC for development of infrared imaging arrays.

IV. Conclusion

In this work, planar InAs APDs were fabricated using Be ion implantation at an energy of 34 keV. Samples with blanket ion implantation were subjected to different post implant annealing conditions. Mesa diodes were fabricated from these samples. A 15 minute anneal at 500 °C was found to be sufficient to yield good diode behavior with bulk dominated dark current at room temperature. Hence, a 15 minute anneal at 500 °C, was used to fabricate planar APDs. Three sets of planar APDs, with no surface treatment, with HF treatment and with a shallow surface etch, were compared. Treatment with HF and a shallow surface etch were observed to reduce the dark current and increase the responsivity. When compared to the untreated planar APDs, the planar APDs with a shallow surface etch were found to have a more pronounced reduction in the dark current density from 1.46 to 0.52 A/cm^2. The responsivity also increases from 0.48 A/W in the untreated planar APDs to 0.62 A/W in the planar APDs with a shallow surface etch. These results show 3 times smaller dark current and 1.4 times greater responsivity compared to previous high energy Be-implanted planar InAs APDs [17].

References

[1] X. Zhou, X. Meng, A. Krysa, J. R. Wilmott, J. S. Ng, and C. H. Tan, "InAs photodiodes for 3.43 μm radiation thermometry," *IEEE Sens. J.*, vol. 15, no. 10, pp. 5555–5560, Oct. 2015.

[2] X. Liu, S. Cheng, H. Liu, S. Hu, D. Zhang, and H. Ning, "A survey on gas sensing technology," *Sensors*, vol. 12, pp. 9635–9665, Jul. 2012.

[3] E. Repasi, P. Lutzmann, O. Steinvall, M. Elmqvist, B. Göhler and G. Anstett, "Advanced short-wavelength infrared range-gated imaging for ground applications in monostatic and bistatic configurations," *Appl. Opt.*, vol. 48, no. 31, pp. 5956–5969, Nov. 2009.

[4] G. A. Howland, P. B. Dixon, and J. C. Howell, "Photon-counting compressive sensing laser radar for 3D imaging," *Appl. Opt.*, vol. 50, no. 31, pp. 5917–5920, Nov. 2011.

[5] J. Beck *et al.*, "The HgCdTe electron avalanche photodiode," *J. Electron. Mater.*, vol. 35, no. 6, pp. 1166–1173, 2006.

[6] X. Sun, J. B. Abshire, J. D. Beck, P. Mitra, K. Reiff, and G. Yang, "HgCdTe avalanche photodiode detectors for airborne and spaceborne lidar at infrared wavelengths," *Opt. Express*, vol. 25, no. 14, pp. 16589–16602, Jul. 2017.

[7] A. Rogalski, "Recent progress in infrared detector technologies," *Infrared Phys. Technol.*, vol. 54, pp. 136–154, Dec. 2010.
[8] W. Lei, R.J. Gu, J. Antoszewski, J. Dell, and L. Faraone, "GaSb: A new alternative substrate for epitaxial growth of HgCdTe," *J. Electron. Mater.*, vol. 43, pp. 2788–2794, Feb. 2014.
[9] J. Beck, T. Welch, P. Mitra, K. Reiff, X. Sun and J. Abshire, "A highly sensitive multi-element HgCdTe e-APD detector for IPDA Lidar applications," *J. Electron. Mater.*, vol. 43, pp. 2970–2977, Aug. 2014.
[10] European Commission, "EU protects citizens from toxic mercury, paves the way for global action," May 2017. [Online]. Available: http://europa.eu/rapid/press-release_IP-17-1345_en.htm. Accessed on: Apr. 19, 2018.
[11] P. J. Ker, J. P. R. David, and C. H. Tan, "Temperature dependence of gain and excess noise in InAs electron avalanche photodiodes," *Opt. Express*, vol. 20, no. 28, pp. 29568–29576, Dec. 2012.
[12] A. R. J. Marshall, P. J. Ker, A. Krysa, J. P. R. David, and C. H. Tan, "High speed InAs electron avalanche photodiodes overcome the conventional gain-bandwidth product limit," *Opt. Express*, vol. 19, no. 23, pp. 23341–23349, Nov. 2011.
[13] S. Butera, P. Vines, C. H. Tan, I. Sandall, and G. S. Buller, "Picosecond laser ranging at wavelengths up to 2.4 μm using an InAs avalanche photodiode," *Electron. Lett.*, vol. 52, no. 5, pp. 385–386, Mar. 2016.
[14] P. J. Ker, A. R. J. Marshall, J. P. R. David and C. H. Tan, "Low noise high responsivity InAs electron avalanche photodiodes for infrared sensing," *Phys. Status Solidi C*, no. 2, pp. 310–313, Dec. 2011.
[15] P. J. Ker, A. R. J. Marshall, A. B. Krysa, J. P. R. David and C. H. Tan, "Temperature dependence of leakage current in InAs avalanche photodiodes," *IEEE J. Quantum Electron.*, vol. 47, no. 8, pp. 1123–1128, Aug. 2011.
[16] A. R. J. Marshall, J. P. R. David, and C. H. Tan, "Impact ionization in inas electron avalanche photodiode," *IEEE Trans. Electron Devices*, vol. 57, no. 10, pp. 2631–2638, Oct. 2010.
[17] C. H. Tan, A. Velichko, L. W. Lim and J. S. Ng, "Few-photon detection using InAs avalanche photodiode," *Opt. Express*, vol. 27, no. 4, pp. 5835–5842, Feb. 2019.
[18] C. P. Skrimshire *et al.*, "Reliability of mesa and planar InGaAs PIN photodiode," *IEE Proc.*, vol. 137, no. 1, pp. 74–78, Feb. 1990.
[19] B. S. White, I. C. Sandall, J. P. R. David, and C. H. Tan, "InAs diodes fabricated using Be ion implantation," *IEEE Trans. Electron Devices*, vol. 62, no. 9, pp. 2928–2932, Sep. 2015.
[20] B. S. White *et al.*, "High-gain InAs planar avalanche photodiode," *J. Lightw. Technol.*, vol. 34, no. 11, pp. 2639–2644, Jun. 2016.
[21] J. F. Ziegler, M. D. Ziegler and J. P. Biersack, "SRIM – the stopping and range of ions in matter," *Nucl. Instrum. Methods Phys. Res.*, vol. 268, pp. 1818–1823, Feb. 2010.
[22] J. R. Dixon and J. M. Ellis, "Optical properties of n-type indium arsenide in the fundamental absorption edge region," *Phys. Rev.*, vol. 123, no. 5, pp. 1560–1566, Sep. 1961.
[23] Y. Nemirovsky and G. Bahir, "Passivation of mercury cadmium telluride surfaces," *J. Vac. Sci. Technol. A.*, vol. 7, pp. 450–459, Apr. 1989.
[24] A. Singh, A. K. Shukla and R. Pal, "High performance of midwave infrared HgCdTe e-avalanche photodiode detector," *IEEE Electron Device Lett.*, vol. 36, no. 4, pp. 360–362, Apr. 2015.
[25] C. E. Hurwitz and J. P. Donnelly, "Planar InSb photodiodes fabricated by Be and Mg ion implantation," *Solid State Electron.*, vol. 18, pp. 753–756, Dec. 1974.
[26] Teledyne Judson Technologies, "Indium arsenide detectors," [Online]. Available: http://www.teledynejudson.com/products/indium-arsenide-detectors. Accessed on: Apr. 19, 2018.
[27] Hamamatsu Photonics, "InAs photovoltaic detector P10090-01," [Online]. Available: http://www.hamamatsu.com/jp/en/P10090-01.html. Accessed on: Apr. 19, 2018.
[28] W. Sun, Z. Lu, X. Zheng, J. C. Campbell, S. J. Maddox, H. P. Nair, and S. R. Bank, "High-gain InAs avalanche photodiodes," *IEEE J. Quantum Electron.*, vol. 49, no. 2, pp. 154–161, Feb. 2013.

Leh Woon Lim received the B.Eng. degree, in electronic and electrical engineering from the University of Sheffield, Sheffield, U.K., in 2016, where he is currently working toward the Ph.D. degree. His current research interests include fabrication and characterization of avalanche photodiodes for mid-infrared applications.

Chee Hing Tan (M'95–SM'17) received the B.Eng. and Ph.D. degrees in electronic engineering from the Department of Electronic and Electrical Engineering, University of Sheffield, Sheffield, U.K., in 1998 and 2002, respectively.

He is currently a Professor of Opto-Electronic Sensors with the Department of Electronic and Electrical Engineering, University of Sheffield. He has extensive experience in the characterization and modeling of high-speed low-noise avalanche photodiodes and phototransistors. His current research interests include single-photon avalanche diodes, mid-infrared photodiodes, quantum-dot infrared detectors, X-ray detectors, ultrahigh-speed avalanche photodiodes, and phototransistors.

Jo Shien Ng (M'99) received the B.Eng. and Ph.D. degrees in electronic engineering from the University of Sheffield, Sheffield, U.K., in 1999 and 2003, respectively.

She is currently a Professor of Semiconductor Devices with the Department of Electronic and Electrical Engineering, University of Sheffield. She was a Royal Society Research Fellow based in the same department between 2006 and 2016. Her research interests include avalanche photodiodes, Geiger-mode avalanche photodiodes, and material characterization.

Jonathan D. Petticrew (S'16) received the M.Phys. degree, in physics from the University of Sheffield, U.K., in 2015, where he is currently working toward the Ph.D. degree on the design and fabrication of single photon detectors.

Andrey B. Krysa graduated from the Moscow Engineering Physics Institute in 1990, and received the Ph.D. degree from the Lebedev Physical Institute, Moscow, Russia, in 1997.

In 1999, he was awarded an Alexander von Humboldt Fellowship and worked the two subsequent years on the problems of II-VI compounds for blue light emitting structures at the Institut für Halbleitertechnik, RWTH Aachen, Aachen, Germany. He is currently a Senior Research Fellow at the EPSRC National Epitaxy Facility, University of Sheffield, U.K., which he joined in 2001. He is concerned with the study of group III arsenides and phosphides, and the development of epitaxial technologies for relevant heterostructures and semiconductor optoelectronic devices.